IOPscience iopscience.iop.org

Home Search Collections Journals About Contact us My IOPscience

Thermal phase behaviour of *N*-alkyl-*N*-methylpyrrolidinium and piperidinium bis(trifluoromethanesulfonyl)imide salts

This article has been downloaded from IOPscience. Please scroll down to see the full text article.

2006 J. Phys.: Condens. Matter 18 10377

(http://iopscience.iop.org/0953-8984/18/46/006)

View the table of contents for this issue, or go to the journal homepage for more

Download details:
IP Address: 129.252.86.83
The article was downloaded on 28/05/2010 at 14:30

Please note that terms and conditions apply.

INSTITUTE OF PHYSICS PUBLISHING JOURNAL OF PHYSICS: CONDENSED MATTER

J. Phys.: Condens. Matter **18** (2006) 10377–10390 doi:10.1088/0953-8984/18/46/006

Thermal phase behaviour of *N*-alkyl-*N*-methylpyrrolidinium and piperidinium bis(trifluoromethanesulfonyl)imide salts

W A Henderson[1], V G Young Jr[2], W Pearson[1], S Passerini[3], H C De Long[4] and P C Trulove[1,5]

[1] Department of Chemistry, US Naval Academy, 572 M Holloway Road, Annapolis, MD 21402, USA
[2] X-Ray Crystallographic Laboratory, Department of Chemistry, University of Minnesota, Minneapolis, MN 55455, USA
[3] Casaccia Research Center, ENEA, Rome 00060, Italy
[4] US Air Force Office of Scientific Research, Arlington, VA 22203, USA

E-mail: trulove@usna.edu

Received 15 May 2006, in final form 21 September 2006
Published 3 November 2006
Online at stacks.iop.org/JPhysCM/18/10377

Abstract

The phases, ion crystal packing and thermal properties of the *N*-alkyl-*N*-methylpyrrolidinium and piperidinium bis(trifluoromethanesulfonyl)imide ($PYR_{1R}TFSI$ and $PIP_{1R}TFSI$ (subscript $R = 1$ for methyl and 2 for ethyl), respectively) salts are compared using powder and single-crystal x-ray diffraction (XRD) and differential scanning calorimetry (DSC). The crystal structure of $PIP_{12}TFSI$ has been determined at 123 K. The salt crystallizes in the triclinic space group $P\bar{1}$ with $Z = 8$. Structural data are also reported for $PYR_{11}TFSI$ at 153 K and $PIP_{12}TFSI$ at 223 K. $PIP_{11}TFSI$ has identical ion crystal packing to the analogous pyrrolidinium salt $PYR_{11}TFSI$. Since increasing the cation alkyl chain length to propyl or butyl ($R = 3$ or 4) reduces the melting point of the salts below room temperature, this study may provide valuable insight into why these pyrrolidinium and piperidinium salts form room-temperature ionic liquids.

1. Introduction

Much attention has recently been devoted to the use of salts with disordered phases as ferroelectric materials [1–3] or solid electrolytes [4, 5]. For a given salt, many variables exist such as which ions become disordered, the temperatures at which this occurs and the mechanisms for the disorder. *N*-alkyl-*N*-methylpyrrolidinium salts ($PYR_{1R}X$) (with

[5] Author to whom any correspondence should be addressed.

 © 2006 IOP Publishing Ltd Printed in the UK

subscript $R = 1$ for methyl and 2 for ethyl) have been reported to have complex phase behaviour with numerous solid–solid phase transitions present leading to various degrees of ion disorder in plastic crystalline phases prior to melting [6–12]. The structures of the ordered, low-temperature phases for $PYR_{11}I$ (phase III) [13] and $PYR_{11}TFSI$ (phase IV) ($TFSI^- = N(SO_2CF_3)_2^-$) [14] have been reported, as have the structures of the $PYR_{12}TFSI$ ordered (phase IV) and disordered (phase III) phases [15].

A comparison of the $PYR_{1R}X$ salts with the analogous *N*-alkyl-*N*-methylpiperidinium salts ($PIP_{1R}X$) enables one to examine how small variations in cation ring structure influence the ion crystal packing and salt thermophysical properties:

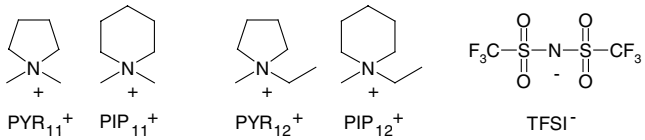

It was recently noted that $PYR_{11}I$ and $PIP_{11}I$ have essentially identical ion crystal packing at 123 K [16]. The thermal behaviour includes a highly endothermic solid–solid phase transition for both salts between 378 and 384 K. Although $PYR_{11}I$ has a second solid–solid phase transition at 478 K, $PIP_{11}I$ does not [16]. It is not yet clear why such differences exist. Here we confirm that the $PYR_{11}TFSI$ and $PIP_{11}TFSI$ salts also have essentially identical crystal packing, but the crystal packing for the $PYR_{12}TFSI$ and $PIP_{12}TFSI$ salts differs at low temperature. Although the melting points (m.p.s) of the $PYR_{11}TFSI/PIP_{11}TFSI$ and $PYR_{12}TFSI/PIP_{12}TFSI$ salts are similar (figures 1 and 2), there are notable differences in the solid–solid phase transitions prior to melting. This thermal behaviour and the nature of the ion disorder in $PIP_{12}TFSI$ are discussed. Powder x-ray diffraction (XRD) has been used to examine and compare the different phases present for these salts. Since the m.p.s of $PYR_{13}TFSI$ and $PIP_{13}TFSI$ are both 286 K, this study may provide valuable insight into the structural reasons as to why certain salts form room-temperature ionic liquids.

2. Experimental details

$PIP_{12}I$ was prepared by combining equimolar amounts of 1-methylpyrrolidine (Aldrich, 97%) and iodoethane (Aldrich, 99.5%) in ethyl acetate. The $PIP_{12}TFSI$ salt was prepared by a metathesis reaction between $PIP_{12}I$ and LiTFSI in deionized water. Both $PIP_{12}I$ and LiTFSI are highly soluble in water, but upon mixing the two solutions, the white solid $PIP_{12}TFSI$ salt crystallizes rapidly. $PIP_{12}TFSI$ was purified by melting the salt in hot deionized water, allowing the solution to cool and the salt to crystallize and then pouring off the water. This was repeated five times. Single crystals were produced as the hot aqueous solution slowly cooled. $PYR_{11}TFSI$, $PYR_{12}TFSI$ and $PIP_{11}TFSI$ salts were prepared in an analogous manner. The salts were dried under high vacuum at 383 K for 24 h and then stored in a N_2 gas controlled atmosphere glove box.

Differential scanning calorimetry (DSC) heating traces were obtained using a TA Model 2910 differential scanning calorimeter calibrated using *n*-heptane, benzene and indium. Hermetically sealed Al pans with the salts were prepared in the glove box. The samples were cooled from room temperature to 133 K, heated to 473 K and then cooled to approximately 143–153 K at 5 K min^{-1}.

A single crystal of $PIP_{12}TFSI$ was placed onto the tip of a 0.1 mm diameter glass fibre and mounted on a Bruker platform CCD diffractometer for data collection. The cryostat on the diffractometer was driven through a sequence of cooling and heating cycles designed to anneal the phase V structure to equilibrium at 123 K: (heating and cooling at

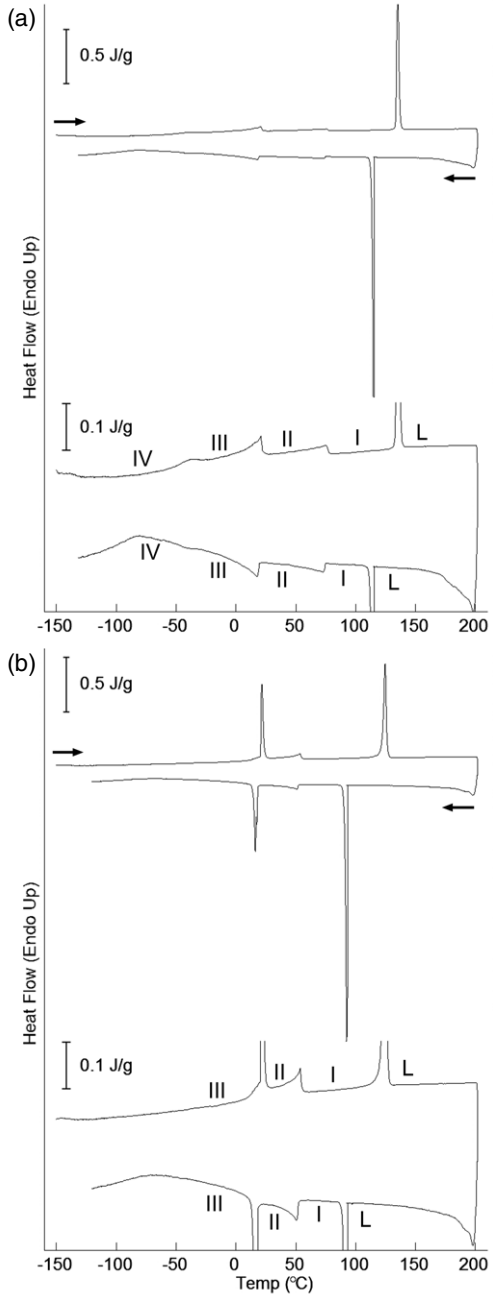

Figure 1. DSC heating and cooling traces (5 K min^{-1}) of (a) $PYR_{11}TFSI$ and (b) $PIP_{11}TFSI$ with the solid (I–IV) and liquid (L) phases indicated (two different resolutions shown).

1 K min^{-1}) 298 K lowered to 173 K, 173 K raised to 253 K, held for 30 min, 253 K lowered to 173 K, 173 K raised to 203 K, and finally 203 K lowered to 123 K and held at 123 K for the duration of the data collection. A preliminary set of cell constants was calculated from reflections harvested from four sets of 50 frames containing 690 reflections.

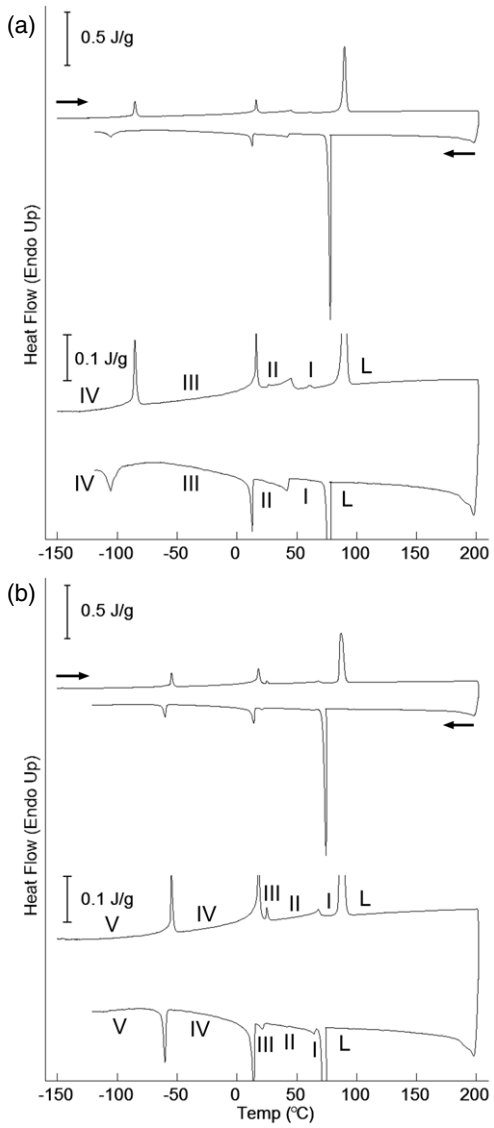

Figure 2. DSC heating and cooling traces (5 K min^{-1}) of (a) $PYR_{12}TFSI$ and (b) $PIP_{12}TFSI$ with the solid (I–V) and liquid (L) phases indicated (two different resolutions shown).

Four twin components by non-merohedry were indexed [17]. The reference component was relatively large, while the other three were relatively small. The mass fractions in descending order are 0.469:0.275:0.164:0.092. The twin law of the second non-merohedral twin component (by rows) is [1 −0.035 −0.124/0 −1 0/0 0 −1], which is a 180° rotation about [100]. The twin law of the third non-merohedral twin component is (by rows) [−1 −0.049 0.050/0.001 −0.051 −0.948/0.000 −1.052 0.052], which is a 180° rotation about $(0\bar{1}1)$. The twin law of the fourth non-merohedral twin component is (by rows) [−1 −0.084 0.077/−0.001 0.052 0.948/0.000 −1.052 −0.051], which is a 180° rotation about [0 1 1].

The data collection was carried out using Mo Kα radiation (graphite monochromator) with a frame time of 30 s and a detector distance of 4.9 cm. A randomly oriented region of reciprocal space was surveyed to the extent of one sphere to a resolution of 0.80 Å. Four major sections of frames were collected with 0.30° steps in ω at four different φ settings and a detector position of $-28°$ in 2θ. Final cell constants were calculated from 2950 strong reflections from the actual data collection after integration (SAINT [18]). The intensity data were corrected for absorption and decay (TWINABS [19, 20]). Redundant reflections in the SHELXTL HKLF 5 data format were removed (Strip_Redundant V1.3 [21]).

The structure was solved and refined using Bruker SHELXTL [22]. The space group $P\bar{1}$ was determined based on systematic absences and intensity statistics. A direct-methods solution was calculated which provided most non-hydrogen atoms from the E-map. Full-matrix least squares/difference Fourier cycles were performed which located the remaining non-hydrogen atoms. All non-hydrogen atoms were refined with anisotropic displacement parameters. All hydrogen atoms were placed in ideal positions and refined as riding atoms with relative isotropic displacement parameters. CCDC 606244 contains the supplementary crystallographic data for the PIP_{12}TFSI phase V. These data can be obtained free of charge via www.ccdc.cam.ac.uk/data_request/cif, by emailing data_request@ccdc.cam.ac.uk, or by contacting the Cambridge Crystallographic Data Centre, 12 Union Road, Cambridge CB2 1EZ, UK; fax: +44 1223 336033.

At the conclusion of the PIP_{12}TFSI phase V data collection at 123 K, the specimen was warmed to 223 K for a data collection of phase IV: (heating and cooling at 1 K min^{-1}) 123 K raised to 233 K, 233 K lowered to 223 K, and held at 223 K for the duration of the data collection. The phase V to phase IV phase transition was observed at 218 K by diffraction as an abrupt event. Data were collected in the same manner as for phase V; however, measurable diffraction intensities were limited to an approximate resolution of 1.05 Å. Indexing revealed a two-component non-merohedral twin in a C-centred monoclinic unit cell approximately twice the volume of the phase V structure (Cell_Now [23]). The conventional C-centred monoclinic unit cell for PIP_{12}TFSI phase IV at 223 K is $a = 28.944(5)$ Å, $b = 17.585(3)$ Å, $c = 13.809(2)$ Å, $\beta = 95.42(2)°$ and $V = 6997(3)$ $Å^3$. The unconventional reduced unit cell is $a = 13.808$ Å, $b = 16.933$ Å, $c = 16.933$ Å, $\alpha = 62.56°$, $\beta = 85.38°$, $\gamma = 85.38°$ and $V = 3498.5$ $Å^3$. This is metrically similar to the phase V structure. The twin law found for the second component of the phase IV structure based on the latter unconventional unit cell is [1 −0.094 −0.092/0 −1 0/0 0 −1], which is a 180° rotation about [100]. This corresponds to the second twin component of phase V; this twinning operation is preserved through the phase transition. The third and fourth twin components are lost concomitantly in the phase V to phase IV phase transition; these twinning operations are converted to new symmetry operations in the C-centred monoclinic unit cell. A preliminary structure was determined on phase IV at 223 K in space group $C2/c$ (SIR-2002) [24]. This result is very poor due to the limiting resolution of the data. It reveals the $Z' = 2$ contents, as expected, with two generally positioned $TFSI^-$ anions, one generally positioned PIP_{12}^+ cation disordered over two closely spaced positions, and two PIP_{12}^+ cations disordered on crystallographic two-fold axes. Given its poor quality due to inherent disorder, no addition information on this structure will be presented here.

For powder XRD measurements, the salts were ground into a fine powder in a mortar and pestle and then sealed in 0.5 mm capillary tubes. Powder data were collected on a Bruker-AXS Smart diffractometer with an Apex-II CCD camera. Variable temperatures were maintained with an Oxford Cryosystems Cobra nitrogen coldstream with stability better than 0.1 K. An uncertainty of 1 K in the reported temperature values reflects the difference between the controller temperature and the real temperature at the crystal position. φ scans were recorded

from 0° to 359° at a fixed χ angle of 54° and 2θ of zero. Scan times were ten minutes per run. The resulting frames were integrated and converted to two-dimensional plots of intensity versus 2θ.

3. Results and discussion

Figures 1–2 show DSC heating/cooling traces and figure 3 shows variable-temperature XRD powder patterns, respectively, for the $PYR_{1R}TFSI$ and $PIP_{1R}TFSI$ salts. These are reproducible during slow thermal cycling of the salts. In general, except as noted below, a comparison of the experimental XRD powder patterns with those calculated from single-crystal structural data (figure 3) shows very good agreement, as expected.

3.1. $PYR_{11}TFSI$ versus $PIP_{11}TFSI$

Although $PYR_{11}TFSI$ and $PIP_{11}TFSI$ have similar melting temperatures, there are notable differences in the phase transitions between the two salts (figure 1). The $PYR_{11}TFSI$ salt appears to have a low-temperature phase IV which is not present for $PIP_{11}TFSI$. In particular, the phase III–II endotherm for the $PYR_{11}TFSI$ salt increases gradually. In contrast, the phase III–II endotherm for $PIP_{11}TFSI$ exhibits a sharp peak (with a gradual onset). For the phase III structure of $PYR_{11}TFSI$, there is a gradual change in the XRD peak intensities (figure 3) and a shift in the peak positions to lower 2θ values with increasing temperatures between 173 and 308 K corresponding to continuous minor structural changes. In contrast, only very minor changes are noted in the peak intensities and positions for the $PIP_{11}TFSI$ phase III structure from 173 to 273 K, but a dramatic transition occurs on further heating to 308 K to form the phase II structure. The phase II to phase I transitions for both $PYR_{11}TFSI$ and $PIP_{11}TFSI$ between 308 and 353 K also occur over a broad temperature range.

A preliminary structure for the $PIP_{11}TFSI$ (phase III) salt at 153 K is shown in figure 4. The refinement of the XRD data for a slowly cooled single crystal (1 K min^{-1}) was poor and only the connectivity for the structure is reported. It is clear that the $PYR_{11}TFSI$ and $PIP_{11}TFSI$ have essentially identical ion crystal packing despite the differences in the cation ring structures. It is not clear, however, why the solid–solid phase transitions differ between the two salts (figure 1). Such transitions most probably arise from the onset of various mechanisms for ion disordering such as rotations of the ions and/or changes in the ion conformations [15]. The slightly different steric environment between the anions and the cation rings may account for the thermal transition differences; for example, the cage created around each cation by the surrounding eight $TFSI^-$ anions may restrict the motion of the PIP_{11}^+ cations more than the PYR_{11}^+ cations. Despite the variations in transition temperatures, it is clear from a comparison of the powder XRD data that the analogous phases for these two salts are essentially isostructural up to the melting transition, explaining the similarity of the m.p. for the two salts.

3.2. $PYR_{12}TFSI$ versus $PIP_{12}TFSI$

In contrast with the dimethyl salts, $PYR_{12}TFSI$ and $PIP_{12}TFSI$ do not have identical crystal packing at low temperature. The crystal structure of $PIP_{12}TFSI$ at 123 K reported here (table 1) consists of an asymmetric unit containing four cations and four anions. Half of the cations and half of the anions are disordered (figures 5 and 6). Copious restraints and constraints were used where deemed necessary. Note that the precision of bond distances for the disordered species in this four-component twin are diminished relative to those not disordered. The percentage occupancy for the ions is: N3 cation (62.1%), N3′ cation (37.9%), N4 cation (59.8%), N4′

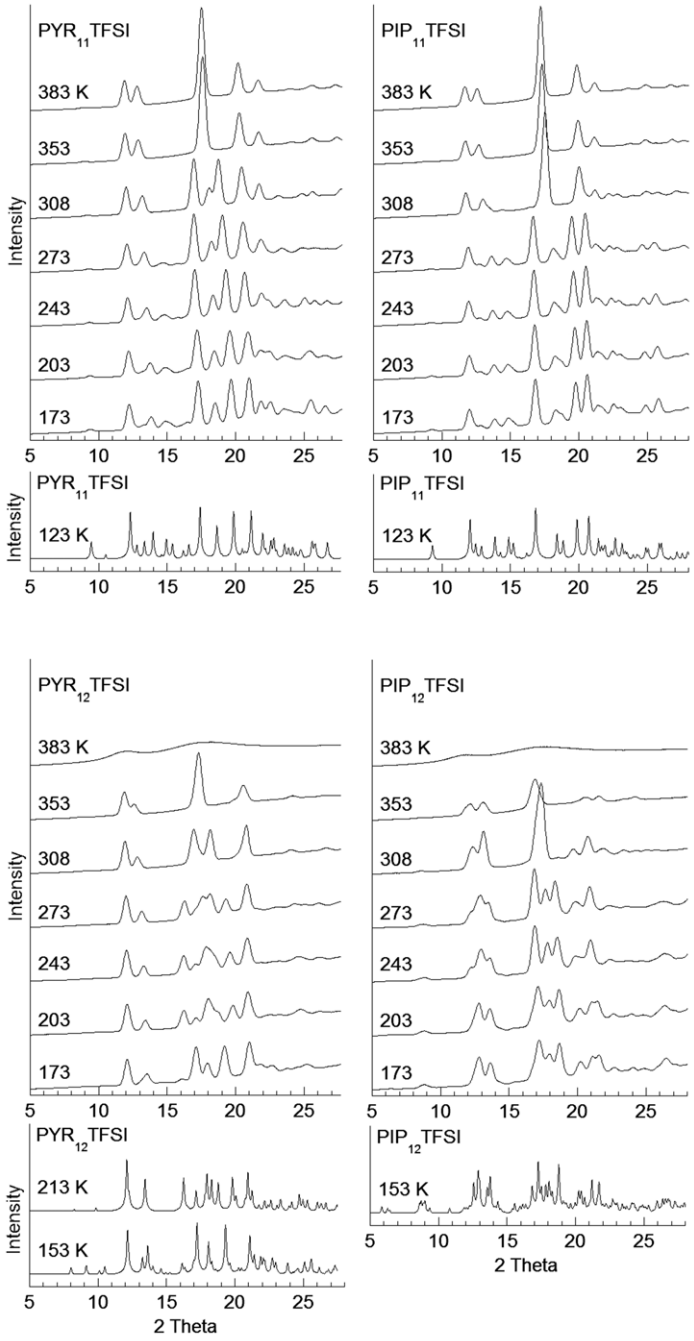

Figure 3. Variable-temperature XRD powder patterns for $PYR_{11}TFSI$, $PIP_{11}TFSI$, $PYR_{12}TFSI$ and $PIP_{12}TFSI$. The XRD powder patterns calculated from single-crystal data are given below each plot for comparison [14, 15].

cation (40.2%), N7 anion (89.8%), N7′ anion (10.2%), N8 anion (58.7%) and N8′ anion (41.3%). The $TFSI^-$ anion is known to have two low-energy conformations with C_1 and C_2

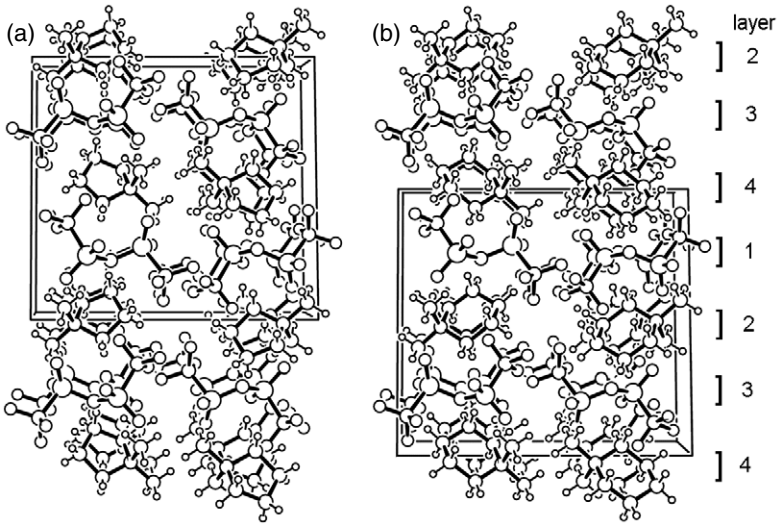

Figure 4. Comparison of the ion crystal packing in (a) $PYR_{11}TFSI$ (phase III) at 123 K [14] and (b) $PIP_{11}TFSI$ (phase III) at 153 K (viewed along the *a*-axis).

Table 1. Crystal data and structure refinement for $PIP_{12}TFSI$.

Empirical formula	$C_{10}H_{18}F_6N_2O_4S_2$
Formula weight	408.38
Temperature (K)	123(2)
Wavelength (Å)	0.71073
Crystal system	Triclinic
Space group	$P\bar{1}$
a (Å)	13.764(5)
b (Å)	16.381(6)
c (Å)	16.861(6)
α (deg)	63.648(4)
β (deg)	85.091(5)
γ (deg)	86.875(5)
Volume (Å^3)	3394(2)
Z	8
ρ_{calc} (g cm^{-3})	1.599
μ (mm^{-1})	0.392
Crystal size (mm)	0.45 × 0.32 × 0.30
F (000)	1680
θ_{max} (deg)	26.37
N (R_{int})	13072 (0.0330)
N [$I > 2\sigma(I)$]	11352
R_1[a], wR_2[b] [$I > 2\sigma(I)$]	0.0426, 0.1034
R_1[a], wR_2[b] (all data)	0.0521, 0.1083
GOF[c]	1.106
$\Delta e_{min,max}$ (e Å^{-3})	−0.457, 0.417

[a] $R_1 = \sum \| F_o | - | F_c \| / \sum | F_o |$.
[b] $wR_2 = [\sum [w(F_o^2 - F_c^2)^2] / \sum [w(F_o^2)^2]]^{1/2}$.
[c] GOF $= [\sum [w(F_o^2 - F_c^2)^2] / (n - p)]^{1/2}$.

symmetry, respectively [25–27]. The C_2 conformation is the norm for crystal structures of salts which do not have coordinated interactions (e.g., hydrogen bonding, ionic bonding, etc)

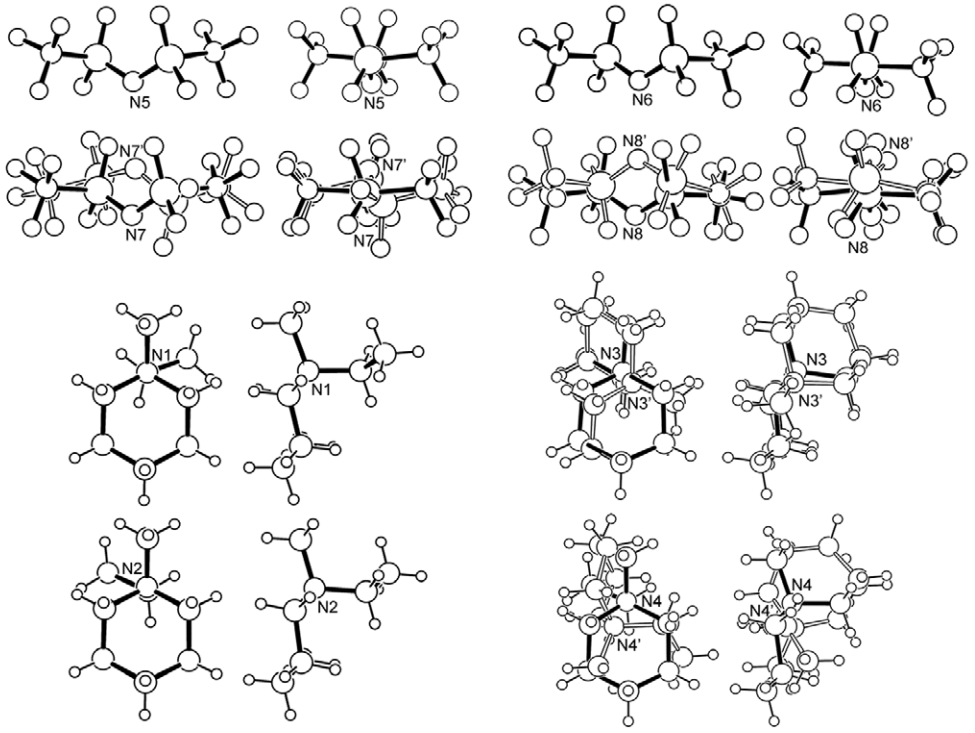

Figure 5. The four cations (N1–N4) and four anions (N5–N8) in the $PIP_{12}TFSI$ structure at 153 K. Two of the anions (N7/N7′ and N8/N8′) and two of the cations (N3/N3′ and N4/N4′) are disordered (two orientations shown for each ion).

between the ions. All of the ions in the $PIP_{12}TFSI$ structure at 123 K have the C_2 structure. The disordered anions, however, have two different C_2 conformations (N7/N7′ and N8/N8′) which are not interchangeable (figure 6). This indicates that the $TFSI^-$ anion transition from one conformation to the other does not arise from the simple rotation of the entire anion. Rather, flexing and rotation of bonds across an inversion centre is required. We have previously reported the same form of $TFSI^-$ anion disorder in crystal structures for Et_4NTFSI [28] and $PYR_{12}TFSI$ (phase III) [15]. It has also been observed for one other salt [29]. A different form of $TFSI^-$ anion disorder has also been recently reported [30].

All of the ions in the $PYR_{12}TFSI$ phase IV structure are ordered, whereas all of the ions are disordered in the $PYR_{12}TFSI$ phase III structure [15]. In the disordered (phase III) structure, in addition to the anion disorder similar to that noted above, the PYR_{12}^+ cation disorder involves both the rotation of the PYR_{12}^+ cation ring and a rotation of the N–C bond for the ethyl group. The cation disorder in the $PIP_{12}TFSI$ salt at 153 K, however, takes a different form. To interchange the disordered cation conformations requires the rotation of the PIP_{12}^+ cation ring, but now the cation ring rotates about a different ion axis resulting in the ring exchanging with the positions previously occupied by the methyl and ethyl groups (figure 6). For one of the disordered cations (N3/N3′), no rotation of the N–C bond for the ethyl group occurs, while such a rotation does occur for the other (N4/N4′) cation. The cations do not have resonance delocalization of the positive charge. Thus, the positive charge is confined principally to the nitrogen atoms which remain in approximately the same position for the two conformations of the disordered cations, resulting in similar electrostatic interactions with

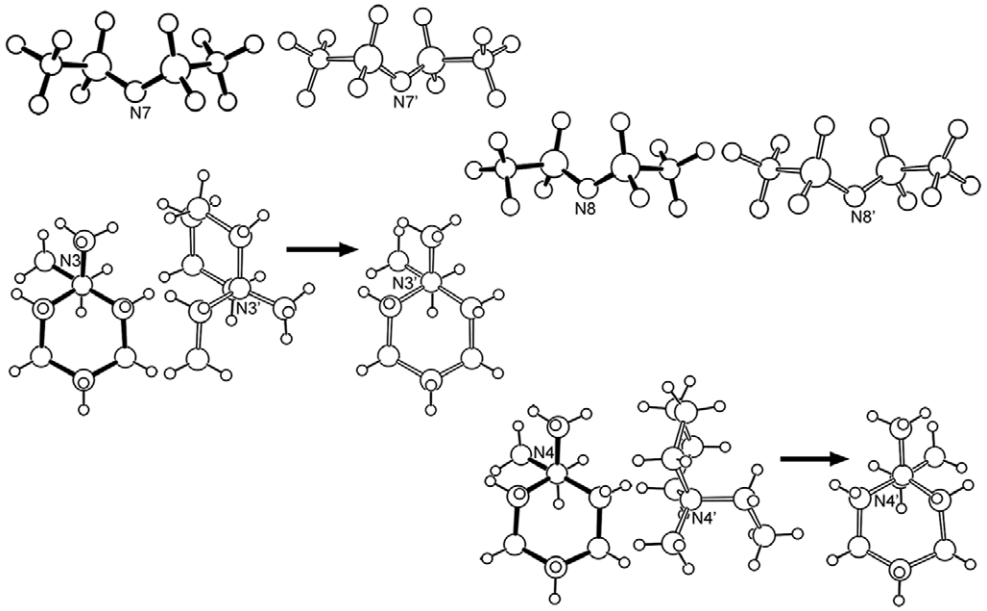

Figure 6. Different orientations of the disordered ions shown in figure 4. The anions with N7′ and N8′ and the cations with N3′ and N4′, respectively, have been reoriented to better compare with the other ions.

the neighbouring anions. This form of overall disordering has been previously reported for *N*-ethyl-*N*-methylmorpholinium ($MORP_{12}^{+}$) cations [31–33].

It is not possible to determine the structures of phase I for the $PYR_{12}TFSI$ and $PIP_{12}TFSI$ salts since the diffraction patterns resemble those of a liquid due to ion disorder. Although the salts differ in ion crystal packing at low temperature, the powder XRD data (figure 3) indicate that the structures are very similar in the disordered phase I at 353 K just prior to melting. In accord with the $PYR_{11}TFSI$ and $PIP_{11}TFSI$ salts, this explains the similarity of the m.p. for $PYR_{12}TFSI$ and $PIP_{12}TFSI$ (figure 2).

3.3. Comparison of ion crystal packing

How does the change from a cation methyl (PYR_{11}^{+}) to an ethyl (PYR_{12}^{+}) group affect the ion crystal packing for the $PYR_{1R}TFSI$ salts? An examination of the structures in figure 4 shows that the ions arrange themselves in layers of anions (layers 1 and 3) and cations (layers 2 and 4). This is true for all of the $PYR_{1R}TFSI$ and $PIP_{1R}TFSI$ ($R = 1$ and 2) salts. Figures 7 and 8 show cutaways from the unit cells of these layers for the different salts (viewed from the top for the salts shown in figure 4). Figure 7 once again clearly shows the identical crystal packing of the ions for $PYR_{11}TFSI$ and $PIP_{11}TFSI$. Each ion fits within a cage of eight counterions (four in the layer above and four below).

It is noteworthy that two of the four anion orientations shown in layers 1 and 3 for the phase IV structure of $PYR_{12}TFSI$ (figure 8(a)) are similar to those in the same layers in $PYR_{11}TFSI$ (figure 7(a)). The remaining anions shown in each layer for $PYR_{12}TFSI$, however, have a different orientation. All of the anions have the C_2 conformation. None of the PYR_{12}^{+} cations, however, have the same orientation as the PYR_{11}^{+} cations.

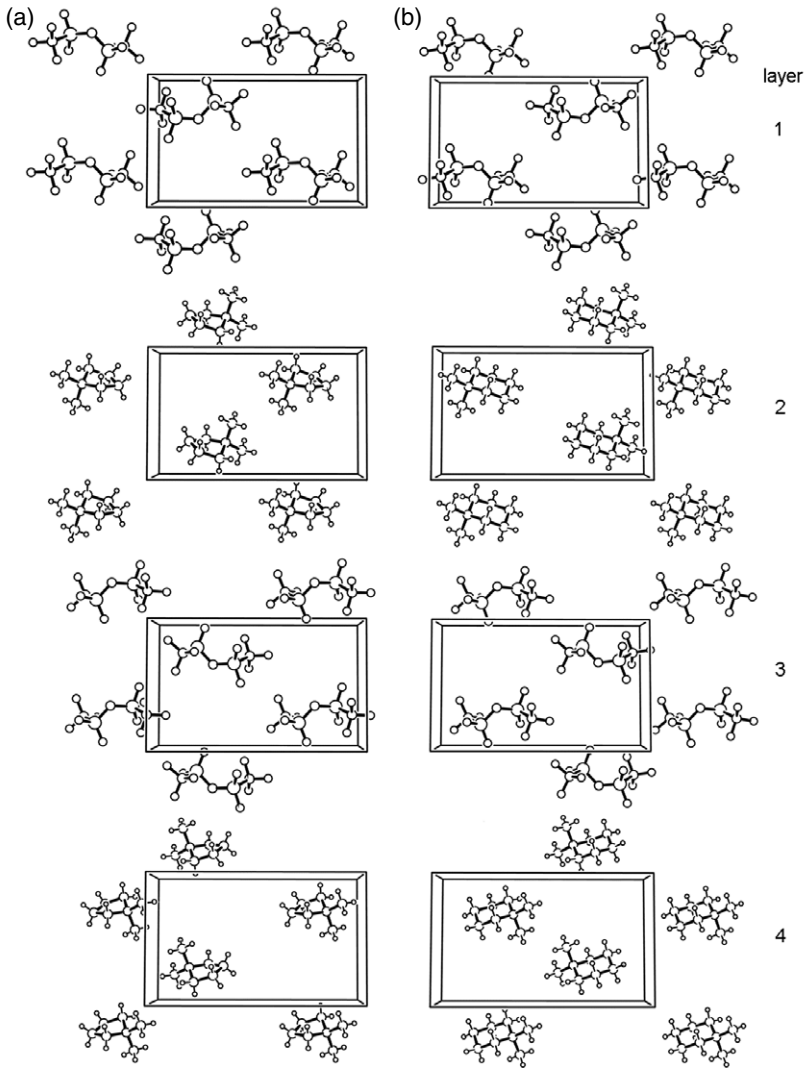

Figure 7. Ion crystal packing for (a) $PYR_{11}TFSI$ (phase IV) at 123 K [14] and (b) $PIP_{11}TFSI$ (phase III) at 153 K. Cutaways for layers of ions (shown in figure 4) viewed from above.

Does the onset of ion disordering in the $PYR_{12}TFSI$ (phase IV to phase III) structure change the overall ion crystal packing? A comparison of 8(a) with figure 8(b) shows that most of the ion orientations in the ordered phase are also present in the disordered phase. The exception is the cations in layer 2. A further comparison with the phase IV structure of $PYR_{11}TFSI$ (figure 7(a)) shows many similarities between the orientations of the $TFSI^-$ anions, indicating the close link between the phase IV structure of $PYR_{11}TFSI$ and the phase IV and III structures of $PYR_{12}TFSI$.

How does the ion crystal packing in the reported $PIP_{12}TFSI$ structure differ from that of $PYR_{12}TFSI$, $PYR_{11}TFSI$ and $PIP_{11}TFSI$? Figure 8(c) shows cutaways of the layers from the unit cell of $PIP_{12}TFSI$. A comparison of layer 1 of the two salts shows differences in the orientations of the ordered anions (figures 8(a) and (c)), but all of the layer 1 anion orientations

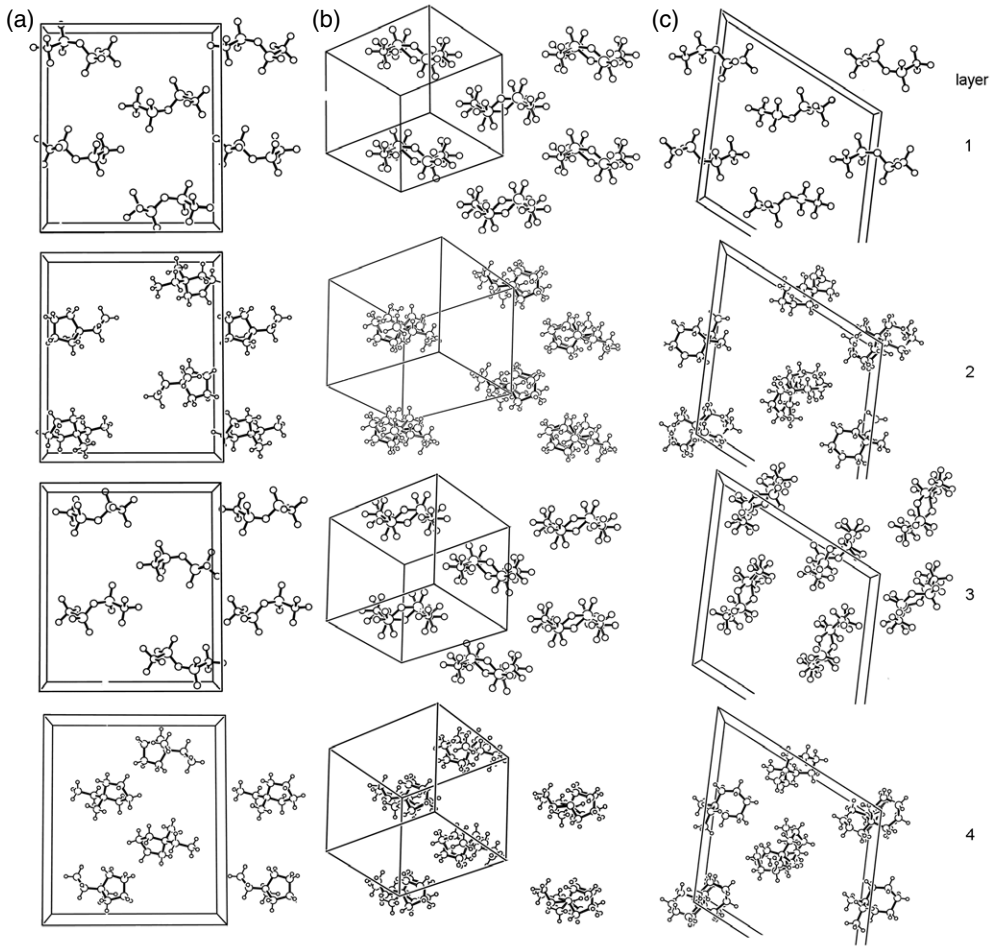

Figure 8. Ion crystal packing for $PYR_{12}TFSI$ (a) (phase IV) at 153 and (phase III) 213 K [15] and (c) $PIP_{12}TFSI$ (phase V) at 153 K. Cutaways for layers of ions viewed from above.

of $PIP_{12}TFSI$ are present in the disordered $PYR_{12}TFSI$ layer 1 (figures 8(b) and (c)). None of the cation orientations in layers 2 and 4 for the two salts are the same. The most dramatic difference, however, is in the disordered anion orientations in layer 3 (figures 8(b) and (c)). The $TFSI^-$ anions have the same form of disorder, but are now rotated from the previous orientations in the other salts. This reorientation of the $TFSI^-$ anions in layer 3 also occurs in the crystal structure of Me_4NTFSI [34].

The disordered phase I structures of the salts are not known, so it is not possible to comment directly on the differences in m.p. for the $PYR_{11}TFSI/PIP_{11}TFSI$ and $PYR_{12}TFSI/PIP_{12}TFSI$ salts. It is interesting to note, however, that the powder XRD data in figure 3 indicate that all of the phase I structures are similar. It seems probable that each solid–solid phase transition enables more degrees of freedom for ionic disordering. Thus, just prior to melting, the ions may be rapidly reorienting and perhaps even isotropically tumbling about equilibrium positions. The minor differences in cation structure would likely not have a significant impact on such chaotic motions and thus the high-temperature structures are very similar.

A similar study of thermal behaviour and crystal packing is now in progress for the $PYR_{1R}TFSI$ and $PIP_{1R}TFSI$ ($R = 3$–5) salts. Note that the crystal structure of $PYR_{14}TFSI$ has recently been reported [35]. The reported m.p. for this salt was 262 K. MacFarlane *et al* noted that $PYR_{14}TFSI$ exhibits a solid–solid phase transition at 249 K and an m.p. at 255 K [36]. Henderson and Passerini, however, reported that this salt exhibits different phase behaviour depending upon its thermal history [37]. If the salt is annealed at 258 K, only a single endotherm is observed indicating an m.p. of 270 K (peak temperature—the onset occurs at 263 K) [37]. Thus, the reported crystal structure is likely for the more thermally stable phase rather than the metastable phase formed on heating the amorphous salt from low temperature.

4. Conclusions

The comparison of the $PYR_{1R}TFSI$ and $PIP_{1R}TFSI$ salts provides a window to view how relatively minor structural modifications to the ions impacts salt thermal properties and crystalline phases. As we have shown, the structural changes may lead only to minor perturbations in the salt solid-state properties or may instead result in major changes. The $PYR_{11}TFSI$ and $PIP_{11}TFSI$ salts have the same ion crystal packing at low temperature, but this is not the case for $PYR_{12}TFSI$ and $PIP_{12}TFSI$. Despite this, the high-temperature disordered phases present before melting do appear to be very similar, explaining the similar m.p.s for the analogous pyrrolidinium and piperidinium salts. The ions undergo various forms of disordering which has been explored with single-crystal structures. This study is very revealing with regard to how the ion structure and thermal properties of a salt are linked and may provide insight into why such salts with longer cation alkyl chains form room-temperature ionic liquids.

Acknowledgments

The crystallographic figures were drawn using Ortep-III [38]. Portions of this work were supported by the US Air Force Office of Scientific Research and the US Naval Academy Research Council. WAH is grateful to the National Science Foundation for the award of an IRFP fellowship (No 0202620). Any opinions, findings and conclusions or recommendations expressed in this material are those of the authors and do not necessarily reflect the views of the National Science Foundation, US Navy or US Air Force.

References

[1] Bednarska-Bolek B, Jakubas R, Medycki W, Nowak D and Zaleski J 2002 *J. Phys.: Condens. Matter* **14** 3129
[2] Medycki W, Świergiel J, Hołderna-Natkaniec K, Jurga K and Jakubas R 2004 *Solid State Nucl. Magn. Reson.* **25** 129
[3] Jakubas R, Bednarska-Bolek B, Zaleski J, Medycki W, Hołderna-Natkaniec K, Zielinski P and Galazka M 2005 *Solid State Sci.* **7** 381
[4] MacFarlane D R, Huang J and Forsyth M 1999 *Nature* **402** 792
[5] Alarco P-J, Abu-Lebdeh Y and Armand M 2004 *Solid State Ion.* **175** 717
[6] MacFarlane D R, Meakin P, Sun J, Amini N and Forsyth M 1999 *J. Phys. Chem.* B **103** 4164
[7] Hill A J, Huang J, Efthimiadis J, Meakin P, Forsyth M and MacFarlane D R 2002 *Solid State Ion.* **154/155** 119
[8] Forsyth S A, Fraser K J, Howlett P C, MacFarlane D R and Forsyth M 2006 *Green Chem.* **8** 256
[9] Efthimiadis J, Annat G J, Efthimiadis J, Forsyth M and MacFarlane D R 2003 *Phys. Chem. Chem. Phys.* **5** 5558
[10] Seeber A J, Forsyth M, Forsyth C M, Forsyth S A, Annat G and MacFarlane D R 2003 *Phys. Chem. Chem. Phys.* **5** 2692
[11] Adebahr J, Forsyth M and MacFarlane D R 2005 *Electrochim. Acta* **50** 3853
[12] Adebahr J, Seeber A J, MacFarlane D R and Forsyth M 2005 *J. Appl. Phys.* **97** 093904
[13] Golding J, Hamid N, MacFarlane D R, Forsyth M, Forsyth C, Collins C and Huang J 2001 *Chem. Mater.* **13** 558

[14] Forsyth C M, MacFarlane D R, Golding J J, Huang J, Sun J and Forsyth M 2002 *Chem. Mater.* **14** 2103
[15] Henderson W A, Young V G Jr, Passerini S, Trulove P C and De Long H C 2006 *Chem. Mater.* **18** 934
[16] Henderson W A, Young V G Jr, Fylstra P, De Long H C and Trulove P C 2006 *Cryst. Growth Des.* **6** 1645
[17] Sheldrick G 2004 CELL_NOW, University of Göttingen
[18] SAINT V7.20. 2001, Bruker Analytical X-Ray Systems. Madison, WI
[19] Sheldrick G 2004 TWINABS V1.07, University of Göttingen
[20] Blessing R 1995 *Acta Crystallogr.* A **51** 33
[21] Brennessell W W and Young V G Jr 2003 Strip_Redundant V1.3, unpublished
[22] SHELXTL V6.12 2000 Bruker Analytical X-Ray Systems, Madison, WI
[23] Sheldrick G 2004 CELL_NOW beta test V3, University of Göttingen
[24] Burla M C, Camalli M, Carrozzini B, Cascarano G L, Giacovazzo C, Polidori G and Spagna R 2003 *J. Appl. Crystallogr.* **36** 1103
[25] Johansson P, Gejji S P, Tegenfeldt J and Lindgren J 1998 *Electrochim. Acta* **43** 1375
[26] Rey I, Johansson P, Lindgren J, Lassègues J C, Grondin J and Servant L 1998 *J. Phys. Chem.* A **102** 3249
[27] Xue L, Padgett C W, DesMarteau D D and Pennington W T 2002 *Solid State Sci.* **4** 1535
[28] Henderson W A, Herstedt M, Young V G Jr, Passerini S, De Long H C and Trulove P C 2006 *Inorg. Chem.* **45** 1412
[29] Schlueter J A, Geiser U, Wang H H, Kini A M, Ward B H, Parakka J P, Daugherty R G, Kelly M E, Nixon P G, Winter R W, Gard G L, Montgomery L K, Koo H-J and Whangbo M-H 2002 *Solid State Chem.* **168** 524
[30] Babai A and Mudring A-V 2005 *Chem. Mater.* **17** 6230
[31] Figgis B N, Sobolev A N, Kepert C J and Kurmoo M 2001 *Acta Crystallogr.* C **57** 991
[32] van Bodegom B 1981 *Acta Crystallogr.* B **37** 857
[33] van Bodegom B and Bosch A 1981 *Acta Crystallogr.* B **37** 863
[34] Henderson W A, Young V G Jr, Passerini S, Trulove P C and De Long H C 2006 unreported data
[35] Choudhury A R, Winterton N, Steiner A, Cooper A I and Johnson K A 2005 *J. Am. Chem. Soc.* **127** 16792
[36] MacFarlane D R, Meakin P, Amini N and Forsyth M 2001 *J. Phys.: Condens. Matter* **13** 8257
[37] Henderson W A and Passerini S 2004 *Chem. Mater.* **16** 2881
[38] Farrugia L J 1997 Ortep-3 for Windows *J. Appl. Cryst.* **30** 565